The Astrophysical Journal, 801:67 (8pp), 2015 March 1 doi:10.1088/0004-637X/801/1/67

THE BINARY MASS TRANSFER ORIGIN OF THE RED BLUE STRAGGLER SEQUENCE IN M30

Y. Xin[1,4], F. R. Ferraro[2], P. Lu[1], L. Deng[1], B. Lanzoni[2], E. Dalessandro[2], and G. Beccari[3]
[1] Key Laboratory of Optical Astronomy, National Astronomical Observatories, Chinese Academy of Sciences, Beijing 100012, China; xinyu@nao.cas.cn.
[2] Dipartimento di Fisica e Astronomia, Universitá degli Studi di Bologna, Viale Berti Pichat 6/2, I-40127 Bologna, Italy
[3] European Southern Observatory, Karl Schwarzschild Strasse 2, D-85748 Garching bei Munchen, Germany
Received 2014 November 16; accepted 2014 December 31; published 2015 March 4

ABSTRACT

Two separated sequences of blue straggler stars (BSSs) have been revealed by Ferraro et al. in the color–magnitude diagram (CMD) of the Milky Way globular cluster M30. Their presence has been suggested to be related to the two BSS formation channels (namely, collisions and mass transfer in close binaries) operating within the same stellar system. The blue sequence was indeed found to be well reproduced by collisional BSS models. In contrast, no specific models for mass-transfer BSSs were available for an old stellar system like M30. Here we present binary evolution models, including case-B mass transfer and binary merging, specifically calculated for this cluster. We discuss in detail the evolutionary track of a 0.9 + 0.5 $M_{\odot}$ binary, which spends approximately 4 Gyr in the BSS region of the CMD of a 13 Gyr old cluster. We also run Monte Carlo simulations to study the distribution of mass-transfer BSSs in the CMD and to compare it with the observational data. Our results show that (1) the color and magnitude distribution of synthetic mass-transfer BSSs defines a strip in the CMD that nicely matches the observed red-BSS sequence, thus providing strong support to the mass-transfer origin for these stars; (2) the CMD distribution of synthetic BSSs never attains the observed location of the blue-BSS sequence, thus reinforcing the hypothesis that the latter formed through a different channel (likely collisions); (3) most (∼60%) of the synthetic BSSs are produced by mass-transfer models, while the remaining <40% requires the contribution from merger models.

Key words: binaries: close – blue stragglers – globular clusters: individual (M30, NGC 7099)

Supporting material: machine-readable table

1. INTRODUCTION

Blue straggler stars (BSSs) are commonly defined as stars brighter and bluer than the main-sequence (MS) turnoff in the host stellar cluster. They are thought to be central H-burning stars, more massive than the MS turnoff stars (Shara et al. 1997; Gilliland et al. 1998; De Marco et al. 2004; Fiorentino et al. 2014). In stellar systems with no evidence of recent star formation, their origin cannot be explained in the framework of normal single-star evolution and two main formation channels are currently favored: (1) mass transfer (MT) in binary systems, possibly up to the complete coalescence of the two stars, and (2) stellar collisions. Both these processes can potentially bring new hydrogen into the core and therefore "rejuvenate" a star to its MS stage (e.g., Lombardi et al. 1995, 2002; Chen & Han 2009).

The scenario of physical collision was originally presented by Hills & Day (1976), and then different colliding encounters including single–single (Benz & Hills 1987), single–binary, and binary–binary processes (Leonard 1989; Ouellette & Pritchet 1998) have been investigated in subsequent work. Collisions are believed to be important especially in dense environments, such as the cores of globular clusters (GCs; Bailyn 1992; Ferraro et al 1995, 1997, 2003a, 2003b) and even the center of some open clusters (Leonard & Linnell 1992; Glebbeek et al. 2008).

McCrea (1964) first proposed that BSSs can be formed through MT in close binaries. The process starts when the primary fills up its Roche lobe and then transfers material to the secondary through the inner Lagrangian point. The secondary increases its mass and shows up as a BSS when its luminosity exceeds that of the MS turnoff stars. There are three cases of MT, defined according to the evolutionary stage of the primary when it starts to transfer mass to the secondary (Kippenhahn & Weigert 1967): case-A when the primary is on the MS, case-B when it is in post-MS but before helium ignition, and case-C during central He burning and thereafter. Tian et al. (2006) reveal that the BSSs in M67 can be effectively generated in short-period binaries via case-A and case-B MT. Lu et al. (2011) pay close attention to BSS populations in the intermediate-age star clusters, where they find that both case-A and case-B MT can produce BSSs, and BSSs via case-B are generally bluer and even brighter than those from case-A. MT in binaries might be the dominant formation channels in all environments (e.g., Knigge et al. 2009; Leigh et al. 2013), and most likely it is so in low-density GCs, open clusters and the Galactic field (Ferraro et al. 2006b; Sollima et al. 2008; Mathieu & Geller 2009; Preston & Sneden 2000). In the case of case-B or case-C binary origin, a BSS with a white dwarf companion is expected. This has been recently confirmed for three objects in the open cluster NGC 188, thanks to *Hubble Space Telescope* (*HST*) ultraviolet observations (Gosnell et al. 2014). MT can also produce anomalous surface composition on the accretor's surface. Indeed C and O depletion has been observed in the atmosphere of a sub-sample of BSSs in the GCs 47 Tucanae, M30, and ω Centauri (Ferraro et al. 2006a; Lovisi et al. 2013; Mucciarelli et al. 2014), thus likely indicating the MT origin of these stars.

Because of their large number of member stars, GCs are the ideal environment for BSS studies. Nominally all the GCs observed so far have been found to harbor a significant number of BSSs (Piotto et al. 2004; Leigh et al. 2007). Moreover, the stellar density in GCs varies dramatically from the central regions to the outskirts, and since BSSs in different environments (low versus high density) could have different origins (e.g., Fusi Pecci

[4] The work is supported by the National Natural Science Foundation of China through grant Y111221001 and the 973 Program 2014CB845702.

et al. 1992; Davies et al. 2004), these stellar systems allow to investigate both formation channels simultaneously. However a clear distinction is hampered by the internal dynamical evolution of the parent cluster (Ferraro et al. 2012). In fact, having masses larger than normal cluster stars, BSSs are affected by dynamical friction, a process that drives the objects more massive than the average toward the cluster center, over a timescale which primarily depends on the local mass density (e.g., Alessandrini et al. 2014). Hence, as the time goes on, heavy objects (like BSSs) orbiting at larger and larger distances from the cluster center are expected to drift toward the core: as a consequence, the radial distribution of BSSs develops a central peak and a dip, and the region devoid of these stars progressively propagates outward.

Ferraro et al. (2012) used this argument to define the so-called "dynamical clock," an empirical tool able to measure the dynamical age of a stellar system from the shape of its BSS radial distribution. This appears indeed to provide a coherent interpretation of the variety of BSS radial distributions observed so far: GCs with a flat BSS radial distribution (Ferraro et al. 2006a; Dalessandro et al. 2008a; Beccari et al. 2011) are dynamically young systems, GCs with bimodal distributions (e.g., Ferraro et al. 1993, 2004; Lanzoni et al. 2007a; Dalessandro et al. 2008b; Beccari et al. 2013, and references therein) are dynamically intermediate-age systems (their actual dynamical age being determined by the distance of the dip of the distribution from the cluster center), and GCs with a single-peaked BSS distribution (Ferraro et al. 1999b; Lanzoni et al. 2007b; Contreras Ramos et al. 2012; Dalessandro et al. 2013) are dynamically old systems. Following this view, in the cluster center we expect a mixed BSS population: collisional BSSs produced by stellar interactions and MT BSSs drifted to the center because of dynamical friction.

A recent discovery has potentially opened the possibility to photometrically distinguish collisional BSSs from MT BSSs in the same cluster. Two well distinct BSS sequences, almost parallel and similarly populated, have been found in the color–magnitude diagram (CMD) of M30 (Ferraro et al. 2009, hereafter F09). Similar features have been detected also in NGC 362 by Dalessandro et al. (2013) and NGC 1261 by Simunovic et al. (2014). The blue-BSS sequence observed in M30 is nicely reproduced by collisional isochrones (Sills et al. 2009) with ages of 1–2 Gyr. In contrast, the red-BSS population is far too red to be consistent with collisional isochrones of any age, while it seems to well correspond to the "low-luminosity boundary" outlined by the MT binary populations simulated by Tian et al. (2006) for the open cluster M67 (with an age of 4 Gyr), once "extrapolated" to the case of a much older (∼13 Gyr) cluster as M30. However, given the large difference in age between these two systems (which implies significantly different mass regimes for their current binary systems and BSSs), such an extrapolation can be risky and it was made only because no specific models of MT binaries were available at that time for the case of M30.

With the aim of finally providing a firm conclusion about the true nature of the red-BSS sequence observed in M30, here we present MT binary models specifically calculated for this cluster. We also used Monte Carlo simulations to study the distribution of synthetic MT BSSs in the CMD. The details of the binary evolution models are described in Section 2. The results of the Monte Carlo simulations are presented and compared with the observations in Section 3. Section 4 gives summary and discussion.

2. THE MODEL OF PRIMORDIAL BINARIES

We use the stellar evolution code originally written by Eggleton (1971, 1972, 1973) and then updated several times (e.g., Han et al. 1994; Pols et al. 1995, 1998) to calculate the evolution of primordial binaries. The detailed description of the version we used can be found in Han et al. (2000) and Lu et al. (2010). In particular, for this work we adopted the radiative opacity of Iglesias & Rogers (1996) and the molecular opacities of Alexander & Ferguson (1994), and conservations in both mass and angular momentum are assumed.

Roche lobe overflow (RLOF) is used as a boundary condition in the code. When RLOF takes place, the MT rate (dm/dt) between the two components is described as

$$\frac{dm}{dt} = \text{const.} \times \max[0, (R_{\rm star}/R_{\rm lobe} - 1)^3], \quad (1)$$

where $R_{\rm star}$ is the radius of the donor (primary star), and $R_{\rm lobe}$ is the effective radius of the corresponding Roche lobe. We use const. $= 500\,M_\odot$ yr^{-1} to keep the RLOF steady. The donor may overfill its Roche lobe, but the condition of $(R_{\rm star}/R_{\rm lobe} - 1) \leqslant 0.001$ must be satisfied (Han et al. 2000). In order to avoid numerical instabilities, the calculation stops if the RLOF is unstable.

We assume the initial orbital eccentricity to be zero ($e = 0$) for all the models. Convective overshooting is not considered as it can barely influence the evolution of low-mass stars (Pols et al. 1998). After all the fundamental ingredients are prepared, instead of simply approximating the major parameters at each time step by interpolating between corresponding evolutionary tracks, we performed the calculation in a more precise way, exactly following the evolution of both components. Eggleton's code provides details for both components of a binary, but it loses the information of the secondary during the RLOF. We made minor modifications to the code, so that the mass-loss history of the donor is recorded, and it is used to compute the subsequent evolution of the accretor. Such a treatment keeps the evolution of both components synchronized. The accreted material from the donor is assumed to be deposited onto the surface of the accretor and instantly distributed homogeneously over its outer layer.

In this work we initially considered both case-A and case-B MT. However we found that most of the case-A MT binaries did not survive until the current cluster age. Moreover, the MT was often unstable, thus making the code stop and preventing us to follow the complete evolutionary paths of these systems. Hence, in the following we focus only on case-B MT (and binary mergers). In any case, BSSs generated by case-A MT have been found to lie on the red side of the case-B locus (Lu et al. 2011), and they are therefore expected to not affect the main result of this work. Given the age and the metallicity of M30 (∼13 Gyr and $Z = 0.0001$), its current turnoff mass is $\sim 0.75\,M_\odot$. Hence, the currently observable BSSs generated from case-B MT in primordial binaries should come from donor stars with initial masses roughly between 0.7 and 1.1 $M_\odot$. We can trace case-B MT only if the donor is evolving along the sub-giant branch when the RLOF occurs. The code stops if it is on the red giant branch phase due to numerical instability. It also stops if the sum of the two components' radius is equal to or larger than the orbital radius, which marks the moment when a merger occurs. As the modifications of internal structure and chemical profile are quite complicated during a merging process and still unclear in knowledge, we consider the merger product as a single star

Table 1
Main Parameters of the Illustrative Binary System ($0.9\,M_\odot + 0.5\,M_\odot$)

Epoch	Age (Gyr)	P (days)	a ($R_\odot$)	Mass ($M_\odot$)	$\log(L/L_\odot)$	$\log(T_{\rm eff})$	X_C	Y_C	$\dot{M}$ ($M_\odot$ yr^{-1})
1	0.0000	0.4345	2.7000	0.9000	−0.0193	3.8108	0.7700	0.2299	0.0
				0.5000	−1.1571	3.6524	0.7700	0.2299	
2	7.5412	0.4345	2.7000	0.9000	0.4826	3.8496	0.0485	0.9514	2.6746×10^{-15}
				0.5000	−1.1356	3.6544	0.7029	0.2970	
3	7.5491	0.3366	2.2772	0.6999	−0.0613	3.7783	0.0481	0.9518	3.1974×10^{-8}
				0.6999	−0.0394	3.7937	0.7086	0.2913	
4	12.7828	1.9555	7.3598	0.2349	0.6213	3.7845	0.0000	0.9999	0.0
				1.1663	0.8375	3.9526	0.0843	0.9157	
5	13.0000	1.9555	7.3598	0.2349	0.7841	4.0965	0.0000	0.9999	0.0
				1.1663	0.8870	3.9564	0.0313	0.9687	

Notes. The columns are (1) reference epoch number, (2) age in Gyr, (3) orbital period in days, (4) separation between the two components, (5) mass in $M_\odot$, (6) luminosity in $\log(L/L_\odot)$, (7) logarithm of the effective temperature, (8) hydrogen mass fraction in the core, (9) helium mass fraction in the core, and (10) MT rate in $M_\odot$ yr^{-1}. The epoch indicates (1) the ZAMS, (2) the beginning of MT, (3) the time when the mass ratio is equal to 1, (4) the end of MT, and (5) the time is equal to 13 Gyr. Two lines in each epoch indicate the parameters of the primary (up) and the secondary (low) components, respectively.

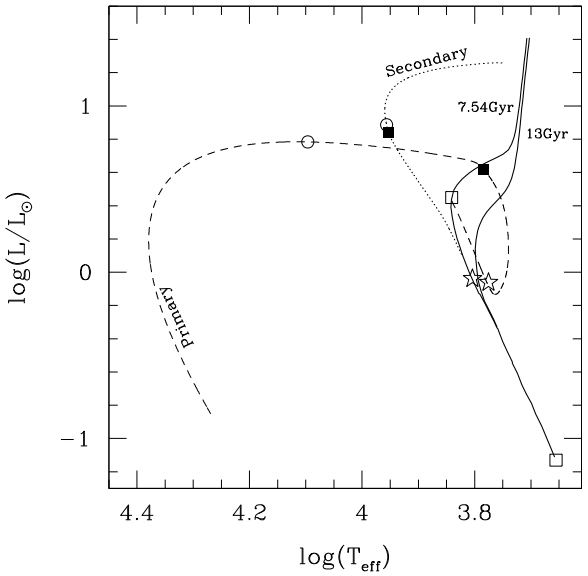

Figure 1. Evolutionary tracks for an illustrative example of binary system ($0.9\,M_\odot + 0.5\,M_\odot$, initial orbital radius $= 2.7\,R_\odot$) undergoing case-B mass transfer (MT). The evolutionary tracks of the primary (donor) and secondary (accretor) stars are shown as dashed and dotted lines, respectively. Different symbols mark a few key events in the binary evolution: the beginning of MT (open squares), the epoch at which the mass ratio is equal to one (open stars), the end of the MT process (solid squares), and the 13 Gyr age (open circles). For the sake of comparison, the 7.54 and 13 Gyr isochrones at the appropriate metallicity of M30 ($Z = 0.0001$) are also plotted in solid lines.

with mass equal to the sum of the two components' masses and evolved from its zero age main sequence (ZAMS) to an age equal to 13 Gyr minus the time of the merger. The hydrogen fuel in its core is calculated as the sum of the central hydrogen left in the two components when merging happens.

As an illustrative example of a binary system experiencing MT and producing a BSS in M30, we calculated a binary with metallicity appropriate for the cluster ($Z = 0.0001$; Ferraro et al. 1999a), composed of a primary (donor) with $0.9\,M_\odot$ and a secondary (accretor) with $0.5\,M_\odot$, and having an initial orbital radius of $2.7\,R_\odot$. Figure 1 shows the evolutionary tracks of the two components (dashed and dotted lines for the primary and the secondary, respectively). Both tracks are interpolated using the time step of the component for which the calculation stops first. We also report a few symbols along the evolutionary tracks to flag reference events in the evolution of the two components: (1) the beginning of the MT process (open squares), (2) the epoch at which the mass ratio (q) is equal to one (open stars), (3) the end of the MT process (solid squares), and (4) the location at 13 Gyr (open circles). It is shown that the two components severely depart from the regular evolutionary tracks after MT begins. Actually, according to case-B MT, the primary is just leaving its MS when the RLOF occurs, at the age of ∼7.54 Gyr (open square along the dashed line). After MT stops at the age of ∼12.78 Gyr (filled square along the dashed line), the primary follows the evolutionary behavior of a single star again and eventually evolves into a white dwarf. In the meanwhile, the secondary gains mass and becomes progressively more luminous. MT stops while the secondary is still in its MS phase (solid square in the dotted line). Both tracks in Figure 1 are truncated at about 1 Gyr after the end of the MT process. As the binary system starts MT at 7.54 Gyr and M30 has an age of 13 Gyr, the corresponding theoretical isochrones are also plotted for reference as solid lines in the figure. Table 1 presents the main parameters of the two components at five key epochs during the binary's evolution.

Of course the photometric properties of the individual components of a binary system cannot be distinguished at the distance of Galactic GCs, and only the combined luminosity of the two components is observed. Hence, in order to perform an appropriate comparison with the observations, for each synthetic BSS we computed the total light as the sum of the luminosities of the two components, at each evolutionary step. To this end, we used our set of models, which describe the properties (e.g., effective temperature, luminosity, mass, and surface gravity) of each component of the binary system along their evolutionary tracks. In particular, from the effective temperature and gravity we constructed synthetic spectrum for each component by linearly interpolating between relevant spectra from the `ATLAS9` library (Castelli & Kurucz 2004). Then, the magnitudes have been obtained by convolving the spectrum with the throughput curves of the photometric filters. Specifically for this work, as the observational data for M30 have been acquired in the *F555W* and *F814W* filters of the WFPC2 on board the *HST*, the throughput curves have been directly downloaded from the `STScI`

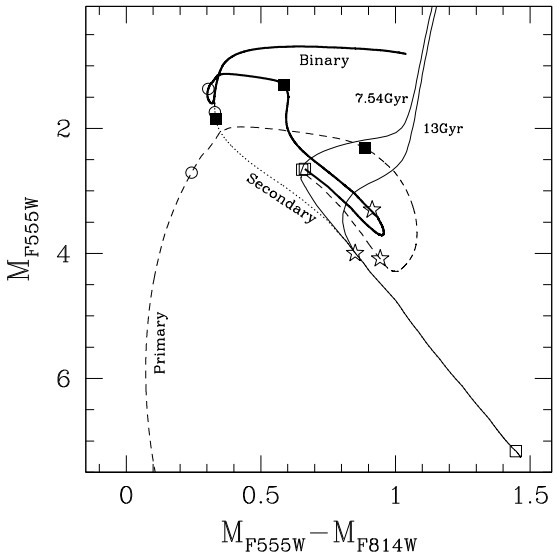

Figure 2. As in Figure 1, but in the absolute CMD and with added the track of the binary system (thick solid line), obtained by combining the luminosity contributions of the primary and secondary components. The two thin solid lines are the 7.54 and 13 Gyr isochrones.

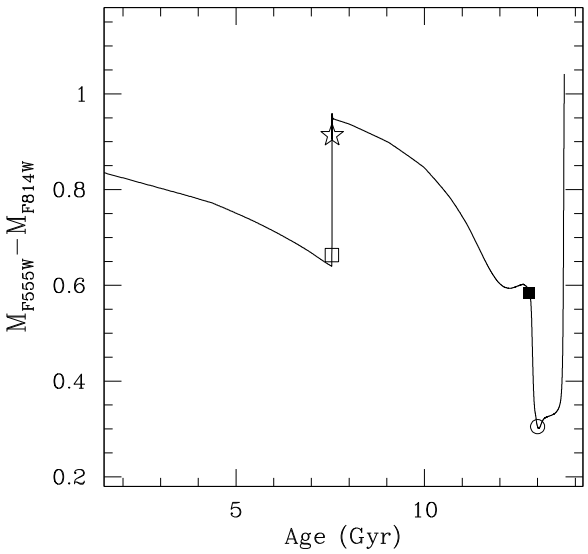

Figure 3. Time evolution of the color of the synthetic binary system considered in Figures 1 and 2. All the symbols keep the same meaning as in the previous figures.

Web site.[5] The zero points have been calculated by making the *V*-band magnitude of Vega equal to 0.03, and all its colors equal to 0.00. Also the Vega spectrum has been extracted from the ATLAS9 library. The synthetic magnitude of two components is calculated with the following formula:

$$M_i = M_{i,1} - 2.5 \times \log\left(1 + 10^{\frac{M_{i,1}-M_{i,2}}{2.5}}\right), \quad (2)$$

where M_i, $M_{i,1}$, and $M_{i,2}$ are the *i*-band magnitudes of the binary, the primary, and the secondary, respectively.

The evolutionary track of the selected binary system in the absolute CMD ($M_{F555W}-M_{F814W}$, M_{F555W}) is presented in Figure 2 in thick solid line. As in Figure 1, the dashed and the dotted lines are the tracks of the primary and the secondary, respectively. The two thin solid lines are the 7.54 and 13 Gyr isochrones. The figure clearly shows that before the inversion of the mass ratio (star symbols), the (higher luminosity) primary component dominates the synthetic track of the binary system, but after that moment, the secondary becomes dominating and the binary system evolves toward the BSS region in the CMD. Figure 3 shows the evolution of the color of the synthetic binary as a function of time. The combined analysis of Figures 2 and 3 suggests that, after a short initial period during which the luminosity of the binary decreases because the (dominant) primary component is losing mass, the system starts to become progressively brighter and bluer with time. At an age of ∼10 Gyr the binary is brighter and bluer than the MS turnoff point of the cluster population, thus finally appearing as a BSS. The system remains in the BSS region of the CMD for the following 3–4 Gyr, before deviating toward the red giant branch.

3. DISTRIBUTION OF SYNTHETIC MT BSSs IN THE CMD

In order to construct a population of synthetic BSSs originated from MT binaries and compare its distribution in the CMD with the observations of M30, we adopted the following procedure.

1. We build a grid of binary evolution models formally including all possible binary systems able to generate a BSS currently observable in M30.
2. We randomly generated a large number of binaries by extracting the values of the three basic parameters characterizing each system (the masses of the two components and the orbital separation) from appropriate distribution functions.
3. For those binaries generated in step (2) and covered by the grid constructed in step (1), we identified their most appropriate stellar models by multi-dimensional interpolation within the grid.
4. All such binaries (from step (3)) that appear to be brighter and bluer than the MS turnoff of M30 have been retained as BSSs and included in what we call the "synthetic BSS reservoir," and that is used for the comparison with the observations.

The following sections provides the details of such a procedure.

3.1. Building Up the Grid of Models

In order to investigate how BSSs originated via MT in primordial binaries populate the CMD of an old GC (as M30), a grid including all the models of primordial binaries that have started MT and/or merging process and can survive at least for 13 Gyr is required. We therefore calculated binary models assuming suitable combinations of their basic parameters, each model (either "pure" MT, or binary merger) representing a node of the grid. As the work focuses on the contribution of case-B MT to the BSS population in a star cluster like M30, and the turnoff mass of a 13 Gyr isochrone is ∼0.75 $M_\odot$, the range of initial mass for the primary is set to 0.7–1.1 $M_\odot$, with steps of 0.1 $M_\odot$. The upper limit, 1.1 $M_\odot$, is used because a binary system with 1.2 $M_\odot$ primary can barely survive 13 Gyr. The initial mass range of the secondary is wider: we use 0.3–1.1 $M_\odot$, with steps of 0.1 $M_\odot$. The lower limit is set by the minimum mass of a secondary that, in 13 Gyr, can experience MT from a primary in the adopted mass range. The orbital separation ranges from 1.0 to 10 $R_\odot$, with intervals of 0.1 $R_\odot$. The ranges set for these three parameters cover all the possibilities of making

[5] http://www.stsci.edu

Table 2
Excerpt from the Grid of Binary Models

Age (Gyr)	$M_{1,g}$ ($M_\odot$)	$M_{2,g}$ ($M_\odot$)	a_g ($R_\odot$)	M_{F555W} (mag)	$M_{F555W} - M_{F814W}$ (mag)
13.0	0.8	0.3	2.8	4.22	0.76
13.0	0.8	0.3	2.9	4.14	0.74
13.0	0.8	0.3	3.0	4.06	0.74
13.0	0.8	0.4	1.9	4.83	0.85
13.0	0.8	0.4	2.0	4.73	0.83
13.0	0.8	0.4	2.1	4.62	0.81
13.0	0.8	0.4	2.2	4.51	0.80
13.0	0.8	0.4	2.3	4.41	0.78
13.0	0.9	0.5	2.0	3.53	0.63
13.0	0.9	0.5	2.1	3.39	0.58

Notes. The columns are (1) current age, (2) initial mass of the primary, (3) initial mass of the secondary, (4) initial orbital separation of the two components, (5) *HST*/WFPC2 *F555W* magnitude of the binary at the indicated age, and (6) *HST*/WFPC2 ($F555W - F814W$) color of the binary at the indicated age.

(This table is available in its entirety in machine-readable form.)

a BSS from a case-B MT binary in an old cluster as M30. Note that in a few cases the code stops because the evolutionary stage is numerically unstable. Thus a few nodes of the grid can be missed. However the adopted interpolation procedure (see Section 3.3) between nearby nodes fully recovers this problem. Table 2 gives an excerpt from the overall grid.

3.2. Generating Binary Systems: Distribution Functions

The basic parameters characterizing a binary system are the masses of the two components (or, equivalently, the total binary mass and the component mass ratio) and the orbital separation. In our procedure, each binary is generated by randomly extracting the initial values of these parameters from the following distribution functions.

1. Assuming the initial mass function of Kroupa et al. (1991), we generate binaries with total mass M (in units of $M_\odot$) extracted from the following function (see also Hurley et al. 2001):

$$M(X) = 0.33 \times \left[\frac{1}{(1-X)^{0.75} + 0.04 \times (1-X)^{0.25}} - \frac{(1-X)^2}{1.04} \right], \quad (3)$$

   where X is a random number uniformly distributed between 0 and 1. The values of $M(X)$ are limited between 0.2 and 100 $M_\odot$, based on the assumption that for "traditional" single star populations, the initial mass coverage ranges between 0.1 and 50 $M_\odot$.
2. The mass ratio distribution for binaries in GCs is still quite controversial. Following Hurley et al. (2001), we adopt a uniform distribution between the following two limits:

$$1 > q > \max\left[\frac{0.1}{M(X) - 0.1}, 0.02(M(X) - 50.0) \right]. \quad (4)$$

   The masses of the two components are then obtained from the total binary mass $M(X)$ and the value of q.
3. For the orbital separation, the flat distribution in $\log a$ assumed by Pols & Marinus (1994) is used here. The minimum size of a corresponds to the value when a ZAMS star fills its Roche lobe. The maximum size is 50 AU.

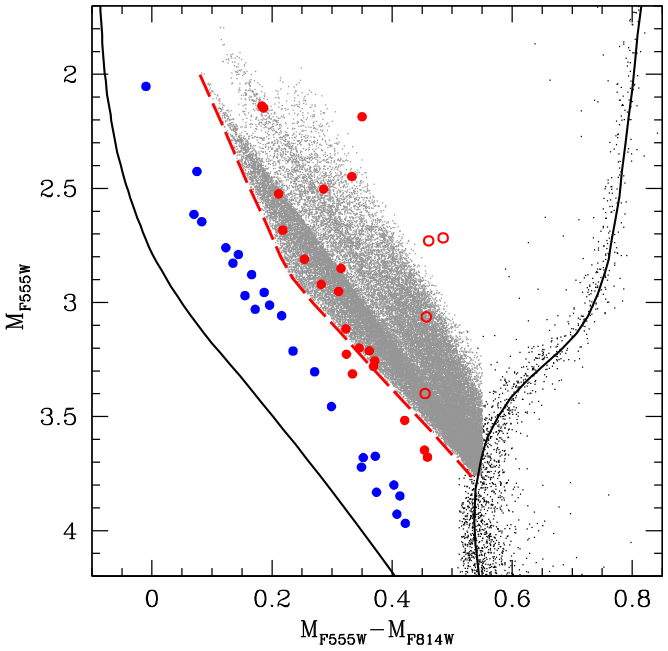

Figure 4. Distribution of the synthetic MT binaries (gray dots) bluer than the cluster MS turnoff, in the absolute CMD of M30. The red dashed line marks the "low-luminosity boundary" of the distribution. The BSSs observed by F09 along the red and the blue sequences are shown as solid red and blue circles, respectively. The positions of four additional red BSSs, not considered in F09, are also shown as empty red circles. Clearly, the distribution of synthetic BSSs well samples the location of the observed red BSSs, and its low-luminosity boundary nicely follows the red-BSS sequence. The black lines, shown for reference, are the 13 Gyr isochrone best fitting the observed M30 data (black dots) and the ZAMS from F09.

3.3. Monte Carlo Simulations: Comparison with the Observations

Monte Carlo simulations were performed by randomly extracting 10^6 values of the binary basic parameters from the distribution functions described in Section 3.2. This provided us with 10^6 binary systems, each characterized by a group of (M_1, M_2, and a) values. Then, the binaries covered by the grid were extracted, and their corresponding stellar evolutionary status at 13 Gyr were determined by means of a multi-dimensional interpolation among the nodes of the grid confining the values of initial M_1, M_2, and a. Since some of the grid nodes are merger models (see Section 3.1), we flag as "merger-important" those binaries for which at least half of the nodes used during the interpolation corresponds to mergers.

For a proper comparison with the observations, we took into account only synthetic binaries that, at the age of 13 Gyr, show photometric properties consistent with the actual definition of BSS in M30, i.e., that appear bluer and brighter than the current location of the cluster MS turnoff point in the CMD. For each Monte Carlo simulation we obtain on average ~15 BSSs, the maximum number being ~44. By performing 2500 such simulations, we thus generated a "reservoir" of more than $\sim 4 \times 10^4$ synthetic BSSs.

Figure 4 shows the distribution of the entire synthetic BSS sample in the CMD of M30. The observed CMD (F09) is transferred into the absolute plane by adopting a distance modulus $(m-M)_V = 14.80$ mag and a color excess $E(V-I) = 0.055$ mag (Ferraro et al. 1999a). Clearly, the distribution of synthetic BSSs (gray dots) well corresponds to the region where the red BSSs of M30 (filled red circles) are observed. According

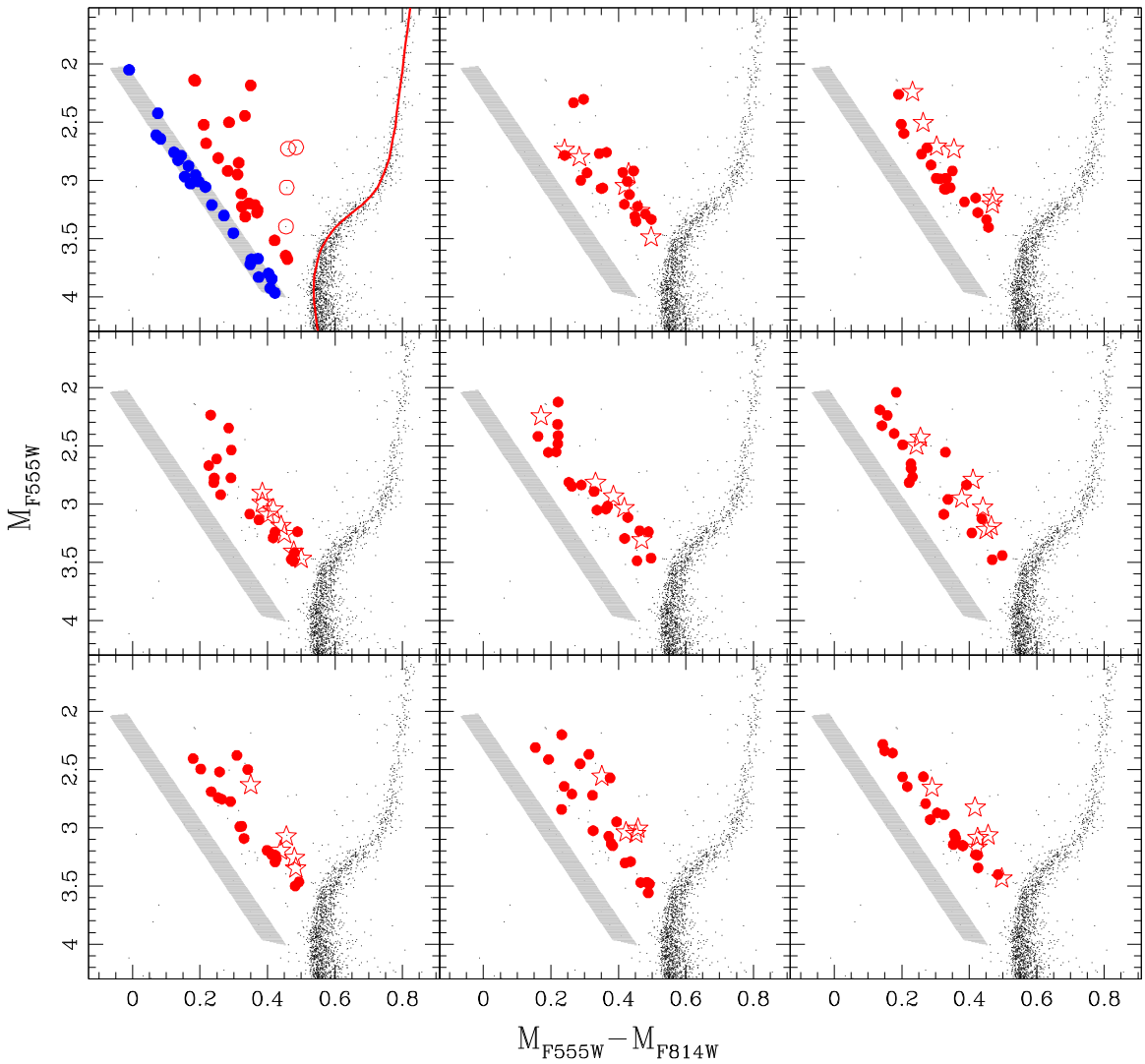

Figure 5. Comparison between the synthetic MT-BSS population and M30 observations, in the absolute CMD. The upper-left panel shows the observations, with all the symbols and the line keeping the same meaning as those in Figure 4. The following 8 panels show the distribution of 8 sub-samples of 25 synthetic MT BSSs, with the red filled circles representing "MT-produced" BSSs, and the red open stars corresponding to "merger-important" BSSs. In all the panels, the gray strip shows the position of the observed blue-BSS sequence.

to the evolutionary tracks shown in Figure 2, the synthetic MT BSSs cover a wide strip in the CMD corresponding to various stages of MT activity during the BSS formation process. For this reason, in this work we added to the observed sample four red BSSs (empty red circles in Figure 4) that were not considered in F09, but turned out to be located in the synthetic MT-BSS region, instead.

Actually, the distribution of the synthetic BSSs shown in Figure 4 can be used to define a sort of "MT-BSS domain" in the CMD, which can be adopted as reference for future studies.[6] While a further extension to the red side (i.e., toward lower surface temperatures) is expected due to the post-MS evolution of BSSs, the distribution shows a well-defined *low-luminosity boundary* (dashed line in Figure 4), similar to that found in Tian et al. (2006). According to F09, this boundary well corresponds to the CMD location of the $Z = 0.0001$ ZAMS shifted by 0.75 in magnitude. Very interestingly, this low-luminosity boundary follows the red side of the gap between the two observed BSS sequences,[7] thus demonstrating that no MT BSSs can reach the location of the blue-BSS sequence. In turn, this provides further support to the fact that the two BSS sequences found in M30 are generated by two distinct formation mechanisms.

The overall distribution of synthetic BSSs shown in Figure 4 provides a nice view of the MT-BSS domain in the CMD of an old star cluster. As the next step, in order to have a more direct comparison with the observations (where 25 BSSs are counted along the red sequence), we performed random extractions of sub-samples of 25 objects from the synthetic MT-BSS reservoir and studied their distribution in the CMD. To evaluate the relative contribution of MT and binary merging to the total population, in this analysis we also distinguished MT-produced BSSs from merger-important BSSs. The results obtained for eight random extractions are shown in Figure 5. For the sake of comparison, the upper-left panel shows the observations, and

[6] Nicely, this region well corresponds to the "MT-BSS domain" empirically defined by Dalessandro et al. (2013) in the case of NGC 362.

[7] Only five red BSSs turned out to be located (slightly) below the MT low-luminosity boundary. This is probably due to photometric uncertainties (as some residual color equation), or stellar variability. Interestingly, at least two of these stars have been classified as W Uma variables by Pietrukowicz & Kaluzny (2004).

the symbols in this panel keep the same meaning as those in Figure 4. The populations of 25 synthetic BSSs are presented in the other 8 panels, where the red solid circles represent MT-produced BSSs, and the red open stars are merger-important BSSs. A gray strip corresponding to the observed blue sequence is also marked for reference in all the panels. As can be seen from Figure 5, the MT-produced BSSs dominate the red population, providing at least 60% of the total observed number in all cases.

4. SUMMARY AND DISCUSSION

M30 is the first star cluster where two distinct sequences of BSSs have been observed and have been interpreted as the result of the two BSS formation channels (F09): blue BSSs are generated by stellar collisions, red BSSs derive from MT activity in close binaries. Indeed the blue sequence was found to be nicely reproduced by collisional isochrones (Sills et al. 2009), while only a preliminary guess about the MT origin for the red BSSs was provided in F09 on the basis of binary evolution models calculated by Tian et al. (2006) for the open cluster M67. In this work we presented binary evolution models specifically computed for M30 and finally provided convincing evidence that the red sequence is indeed populated by MT BSSs.

We calculated a grid of binary evolution models covering the parameter space (in terms of masses of the components and orbital separation) appropriate for the BSSs currently observed in M30 (age = 13 Gyr and $Z = 0.0001$). We used Monte Carlo simulations to randomly generate large numbers of binary systems, we extracted those binaries that can be covered by the grid, we got their physical and photometric properties at 13 Gyr by interpolating within the model grid, and finally we obtained a "reservoir" of synthetic BSSs by taking into account all the grid-covered MT binaries that are bluer and brighter than the MS turnoff of M30. The distribution of these objects in the CMD has been compared to the observed location of the blue- and red-BSS sequences. Random extractions of 25 such BSSs from the overall reservoir have been used to investigate the relative importance of MT and merger processes for the formation of BSSs. The main results can be summarized as follows.

1. The distribution in the CMD of the synthetic MT BSSs is consistent with the location of the observed red sequence in M30 and never reaches the region occupied by the blue BSSs. This evidence demonstrates that MT processes are unable to produce such "blue" objects. The result also supports the suggestion (F09) that the two parallel sequences observed in M30 are indeed formed by BSSs generated by the two distinct formation channels.
2. Random extractions of 25 synthetic binary BSSs (the same number of observed red BSSs) show that the models always nicely reproduce the observed red sequence.
3. MT-produced BSSs contribute to at least 60% of the total sample, while the remaining <40% BSSs may require assistance from binary mergers.

Of course, the BSS formation mechanisms are far more complex than those investigated in the present paper. In fact, the internal dynamical evolution of GCs certainly plays a significant role in mixing BSSs generated by the different channels, especially in the cluster cores. Hence, distinguishing the two populations is not an easy task. In M30 and a few additional clusters (NGC 362 and NGC 1261; see Dalessandro et al. 2013 and Simunovic et al. 2014, respectively), two populations of BSSs appear separated by a gap in the CMD, thus opening the possibility to investigate them in more details. Indeed the evidence collected to date and the work presented here suggest that this is a very promising way to distinguish collisional from MT BSSs. However, as pointed out in F09, the GCs in which the BSS populations are distinguishable can be rare, since the gap separating the two sub-populations is not a permanent feature. In fact, the future evolution of the BSSs currently observed along the blue sequence will move these stars toward the red in the CMD, thus cleaning up the gap in a few Gyr. For this reason, a recent burst of collisions (possibly driven by the collapse of the core) has been suggested to be at the origin of the tiny and well distinct blue sequence observed in M30 (F09). Thoughtful *N*-body calculations, including internal cluster dynamical evolution, are needed to further investigate the properties of the BSS populations in GCs and better clarify the physical processes that play the most relevant roles in shaping their observed characteristics.

Y.X. is grateful to Dr. Stephen Justham for the suggestive discussions. Y.X. also thanks the National Natural Science Foundation of China for its support through grant Y111221001, and thanks the 973 Program 2014CB845702. This research is part of the project *Cosmic-Lab* (Web site: http://www.cosmic-lab.eu) funded by the European Research Council (under contract ERC-2010-AdG-267675). We thank the anonymous referee for useful suggestions.

REFERENCES

Alessandrini, E., Lanzoni, B., Miocchi, P., Ciotti, L., & Ferraro, F. R. 2014, ApJ, 795, 169
Alexander, D. R., & Ferguson, J. W. 1994, ApJ, 437, 879
Bailyn, C. 1992, ApJ, 392, 519
Beccari, G., Dalessandro, E., Lanzoni, B., et al. 2013, ApJ, 776, 60
Beccari, G., Sollima, A., Ferraro, F. R., et al. 2011, ApJL, 737, L3
Benz, W., & Hills, J. G. 1987, ApJ, 323, 614
Castelli, F., & Kurucz, R. L. 2004, arXiv:astro-ph/0405087
Chen, X. F., & Han, Z. W. 2009, MNRAS, 395, 1822
Contreras Ramos, R., Ferraro, F. R., Dalessandro, E., Lanzoni, B., & Rood, R. T. 2012, ApJ, 748, 91
Dalessandro, E., Ferraro, F. R., Massari, D., et al. 2013, ApJ, 778, 135
Dalessandro, E., Lanzoni, B., Ferraro, F. R., et al. 2008a, ApJ, 681, 311
Dalessandro, E., Lanzoni, B., Ferraro, F. R., et al. 2008b, ApJ, 677, 1069
Davies, M. B., Piotto, G., & de Angeli, F. 2004, MNRAS, 349, 129
De Marco, O., Lanz, T., Ouellette, J. A., Zurek, D., & Shara, M. M. 2004, ApJL, 606, L151
Eggleton, P. P. 1971, MNRAS, 151, 351
Eggleton, P. P. 1972, MNRAS, 156, 361
Eggleton, P. P. 1973, MNRAS, 163, 279
Ferraro, F. R., Beccari, G., Dalessandro, E., et al. 2009, Natur, 462, 1028 (F09)
Ferraro, F. R., Beccari, G., Rood, R. T., et al. 2004, ApJ, 603, 127
Ferraro, F. R., Fusi Pecci, F., & Bellazzini, M. 1995, A&A, 294, 80
Ferraro, F. R., Lanzoni, B., Dalessandro, E., et al. 2012, Natur, 492, 393
Ferraro, F. R., Messineo, M., Fusi Pecci, F., et al. 1999a, AJ, 118, 1738
Ferraro, F. R., Paltrinieri, B., Fusi Pecci, F., et al. 1997, A&A, 324, 915
Ferraro, F. R., Paltrinieri, B., Rood, R. T., & Dorman, B. 1999b, ApJ, 522, 983
Ferraro, F. R., Pecci, F. F., Cacciari, C., et al. 1993, AJ, 106, 2324
Ferraro, F. R., Possenti, A., Sabbi, E., et al. 2003a, ApJ, 595, 179
Ferraro, F. R., Sabbi, E., Gratton, R., et al. 2006a, ApJL, 647, L53
Ferraro, F. R., Sills, A., Rood, R. T., Paltrinieri, B., & Buonanno, R. 2003b, ApJ, 588, 464
Ferraro, F. R., Sollima, A., Rood, R. T., et al. 2006b, ApJ, 638, 433
Fiorentino, G., Lanzoni, B., Dalessandro, E., et al. 2014, ApJ, 783, 34
Fusi Pecci, F., Ferraro, F. R., Corsi, C. E., Cacciari, C., & Buonanno, R. 1992, AJ, 104, 1831
Gilliland, R. L., Bono, G., Edmonds, P. D., et al. 1998, ApJ, 507, 818
Glebbeek, E., Pols, O. R., & Hurley, J. R. 2008, A&A, 488, 1007
Gosnell, N. M., Mathieu, R. D., Geller, A. M., et al. 2014, ApJL, 783, L8
Han, Z. W., Podsiadlowski, P., & Eggleton, P. P. 1994, MNRAS, 270, 121
Han, Z. W., Tout, C. A., & Eggleton, P. P. 2000, MNRAS, 319, 215
Hills, J., & Day, C. 1976, ApJL, 17, 87
Hurley, J. R., Tout, C. A., Aarseth, S. J., & Pols, O. R. 2001, MNRAS, 323, 630

Iglesias, C. A., & Rogers, F. J. 1996, ApJ, 464, 943
Kippenhahn, R., & Weigert, A. 1967, ZA, 65, 251
Knigge, C., Leigh, N., & Sills, A. 2009, Natur, 457, 288
Kroupa, P., Tout, C. A., & Gilmore, G. 1991, MNRAS, 251, 293
Lanzoni, B., Dalessandro, E., Perina, S., et al. 2007a, ApJ, 670, 1065
Lanzoni, B., Sanna, N., Ferraro, F. R., et al. 2007b, ApJ, 663, 1040
Leigh, N., Knigge, C., Sills, A., et al. 2013, MNRAS, 428, 897
Leigh, N., Sills, A., & Knigge, C. 2007, ApJ, 661, 210
Leonard, P. J. T. 1989, AJ, 98, 217
Leonard, P. J. T., & Linnell, A. P. 1992, AJ, 103, 1928
Lombardi, J. C., Jr., Rasio, F. A., & Shapiro, S. L. 1995, ApJL, 445, L117
Lombardi, J. C., Jr., Warren, J. S., Rasio, F. A., Sills, A., & Warren, A. R. 2002, ApJ, 568, 939
Lovisi, L., Mucciarelli, A., Lanzoni, B., et al. 2013, ApJ, 772, 148
Lu, P., Deng, L.-C., & Zhang, X.-B. 2010, MNRAS, 409, 1013
Lu, P., Deng, L.-C., & Zhang, X.-B. 2011, RAA, 11, 1336
Mathieu, R. D., & Geller, A. M. 2009, Natur, 462, 1032
McCrea, W. H. 1964, MNRAS, 128, 147
Mucciarelli, A., Lovisi, L., Ferraro, F. R., et al. 2014, ApJ, 797, 43
Ouellette, J. A., & Pritchet, C. J. 1998, AJ, 115, 2539
Pietrukowicz, P., & Kaluzny, J. 2004, AcA, 54, 19
Piotto, G., De Angeli, F., King, I. R., et al. 2004, ApJL, 604, L109
Pols, O. R., & Marinus, M. 1994, A&A, 288, 475
Pols, O. R., Schroder, K.-P., Hurley, J. R., Tout, C. A., & Eggleton, P. P. 1998, MNRAS, 298, 525
Pols, O. R., Tout, C. A., Eggleton, P. P., & Han, Z. W. 1995, MNRAS, 274, 964
Preston, G. W., & Sneden, C. 2000, AJ, 120, 1014
Shara, M. M., Saffer, R. A., & Livio, M. 1997, ApJL, 489, L59
Sills, A., Karakas, A., & Lattanzio, J. 2009, ApJ, 692, 1411
Simunovic, M., Puzia, T. H., & Sills, A. 2014, ApJL, 795, L10
Sollima, A., Lanzoni, B., Beccari, G., Ferraro, F. R., & Fusi Pecci, F. 2008, A&A, 481, 701
Tian, B., Deng, L.-C., Han, Z.-W., & Zhang, X.-B. 2006, A&A, 455, 247